

ZH Production in Gluon Fusion at NLO

Stephen P. Jones^{a,*}

^a*Institute for Particle Physics Phenomenology, Durham University, Durham DH1 3LE, UK*

E-mail: s.jones@cern.ch

We summarise the calculation of the two-loop next-to-leading order QCD corrections to Z boson plus Higgs boson production in gluon fusion. The result presented includes full top-quark mass effects and is obtained by combining two-loop virtual contributions computed numerically, using sector decomposition, with virtual contributions obtained in a high-energy expansion. We find that the corrections enhance the cross-section by approximately a factor of 2 and reduce the renormalisation and factorisation scale uncertainty by around 30%. For a centre of mass energy of $\sqrt{s} = 13.6$ TeV we obtain

$$\sigma_{gg \rightarrow ZH}^{\text{NLO}(m_t^{\text{OS}})} = 114.7(3)_{-13.7\%}^{+16.2\%} \text{ fb.}$$

We also observe that the choice of top-quark mass renormalisation scheme can have a significant impact on the prediction.

*Loops and Legs in Quantum Field Theory - LL2022,
25-30 April, 2022
Ettal, Germany*

*Speaker

1. Introduction

The production of a Higgs boson in association with a Z boson is an important channel for studying the properties of the Higgs boson at the LHC. The channel receives contributions from diagrams in which the Higgs boson couples to a fermion line and from diagrams in which the Higgs boson couples to a Z boson. It is therefore sensitive to the coupling of the Higgs boson both to fermions and to Z bosons. The channel was recently used to place limits on the Higgs boson coupling to charm quarks [1–3], with the leptonically decaying W/Z boson used to tag the signal events. The ZH channel was also used to observe the Higgs boson decay to bottom quarks [4, 5]. Furthermore, due to the interference between diagrams involving a top-quark Yukawa coupling and diagrams containing a HZZ coupling, the $pp \rightarrow ZH$ process is useful for constraining the sign of the top quark Yukawa and its CP structure [6–9].

The loop-induced $gg \rightarrow ZH$ channel was first calculated at leading order, including the full quark mass dependence, over 30 years ago [10, 11]. The next-to-leading order corrections were computed in the heavy top-quark limit around two decades later [12], these approximate results suggested that the NLO corrections could be very significant, i.e. roughly as large as the LO result. Subsequently, the virtual corrections, which constitute the most challenging piece of the higher-order corrections, were computed in an expansion around large top-quark mass (to $1/m_t^8$) and improved by fitting a Padé approximant [13]. More recently, the virtual corrections were computed in a high-energy expansion (to m_t^3) and Padé [14] improved, and also in full using a numerical approach based on sector decomposition [15]. A NLO result for $gg \rightarrow ZH$ based on a small- m_Z and m_H expansion, but retaining the full top-quark mass dependence, has previously been presented in Ref. [16]. Results for the virtual corrections are also known in an expansion around small- p_T (to p_T^4) [17] and have been combined with the high-energy results [18], a NLO result based on this combination was recently presented in Ref. [19].

The gluon induced channel formally enters at next-to-next-to-leading (NNLO) order for the $pp \rightarrow ZH$ process. However, due to the large gluon luminosity at the LHC, it contributes around 6% of the total NNLO cross section and is significant also in the boosted Higgs regime ($p_T^H \gtrsim 150$ GeV) [6, 12, 20–22]. At LO the gluon induced channel has a large, $O(100\%)$, scale dependence and is a significant source of theoretical uncertainty for ZH production at the LHC [2, 4, 5, 23–27], this motivates the computation of the NLO QCD corrections to the gluon induced channel, which formally contribute to $pp \rightarrow ZH$ at order N^3LO .

Here, we present the full NLO QCD results for the $gg \rightarrow ZH$ process. The two-loop virtual amplitude was obtained by extending the high-energy expansion of Ref. [14] and combining it with the full numerical result of Ref. [15]. The Born and real amplitudes were obtained using the GoSam [28, 29] automated one-loop provider. This work was originally described in Ref. [30].

These proceedings are organised as followed. In Section 2 we briefly describe the setup of the calculation and improvements made to the virtual amplitudes since their original publication. In Section 3 we present results for the total cross section and selected distributions for the ZH invariant mass and transverse momentum. In Section 4 we summarise the results of this work and outline some open issues.

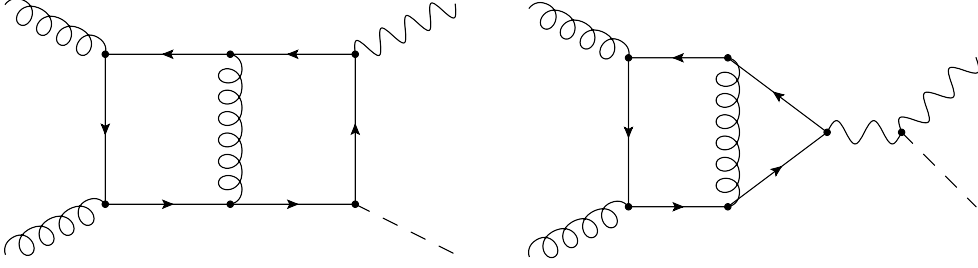


Figure 1: Representative Feynman diagrams for the virtual correction to the $ggZH$ amplitude. We calculate in the Feynman gauge and so also include the set of diagrams where the Z -boson propagators are replaced by Goldstone bosons.

2. Setup

2.1 Virtual amplitude

The most involved step in the calculation of the NLO QCD corrections to $gg \rightarrow ZH$ is in obtaining the two-loop renormalised and infrared (IR) subtracted two-loop virtual amplitude. In this work, our virtual amplitude is based on a combination of the full numerical result of Ref. [15] and the high-energy expansion of Ref. [14].

In Ref. [14], the two-loop amplitude is obtained in an expansion around large and small top-quark mass. In this work only the high-energy (or small top-quark mass) expansion is used. The high-energy expansion is obtained assuming that $m_H^2, m_Z^2 \ll m_t^2 \ll s, |t|$, a Padé approximant is then fitted to improve the convergence of the expansion. Originally, the expansion was computed up to order (m_Z^2, m_H^2, m_t^{32}) . For the virtual amplitude used here, the expansion was extended up to quartic order (m_Z^4, m_H^4, m_t^{32}) including the mixed quartic term $m_Z^2 m_H^2$. In order to assess the reliability of the expansion, we compare it at the level of individual phase-space points to the (more expensive to evaluate) full result. Using only the quadratic terms of the expansion, a difference at the 2 permille level remains between the full and expanded results even at large p_T . Including the quartic terms in the expansion was found to improve the agreement with the full numerical results significantly, with most points at $p_T > 200$ GeV agreeing within the numerical uncertainty at the $2 \cdot 10^{-5}$ level. For our main results we use the high-energy expansion for $p_T > 200$ GeV and the full numerical evaluation for $p_T < 200$ GeV. For the study of the top-quark mass renormalisation scheme, only the high-energy expansion is used, for our choice of cuts, this requires some phase-space points with $150 \text{ GeV} < p_T < 200 \text{ GeV}$, which agree with the numerical virtual amplitude at the level of a few percent.

To optimise our phase-space sampling, we first compute the Born result using Monte-Carlo sampling and a VEGAS grid. We then apply the accept-reject method to Born phase-space points in order to obtain a list of sampling points for the virtual contribution, distributed such that they sample well the product of the gluon-gluon luminosity, the Born matrix element squared and the phase-space factor. An additional weighting function, $f(p_T, m_{ZH})$, is then used to enhance the number of sampling points in specific regions. We use three different sets of sampling points: optimised for the total cross section with $f(p_T, m_{ZH}) = 1$, distributed uniformly in invariant mass with $f(p_T, m_{ZH}) \propto d\sigma_B/dm_{ZH}$ and uniform in p_T with $f(p_T, m_{ZH}) \propto d\sigma_B/dp_T$. We have

evaluated a total of 1294 points for the full numerical result and we combine these results with sets containing an additional 6000 points, optimised for the corresponding distribution, evaluated using the high-energy expansion.

2.2 Real radiation

The real/real-virtual corrections to the Drell-Yan-like and gluon induced $pp \rightarrow ZH$ channels are not completely distinct and there is, therefore, some freedom regarding which gauge invariant sets of diagrams are included/excluded in the gluon-induced corrections. For our $gg \rightarrow ZH$ calculation we include (the gauge invariant set of) all diagrams appearing in the $ggZHg$ and $q\bar{q}ZHg$ amplitudes (and their crossings) which contain a closed fermion loop and have either a Z -boson or a Goldstone boson coupled to that loop. We consider $n_f = 5$ massless quarks and a massive top-quark running in the fermion loops.

For the evaluation of our real radiation matrix elements we use the automated one-loop provider GoSam [28, 29] together with an in-house C++ code, similar to the one used to evaluate $pp \rightarrow HH$ [31, 32]. The IR singularities are subtracted using Catani-Seymour dipole subtraction [33]. To ensure that our real matrix elements are numerically stable, we recompute each point after performing an azimuthal rotation about the beam axis and switch to quadruple precision if the original and rotated results do not agree to 10 digits.

3. Results

We present results using the NNPDF31_nlo_pdfas parton distribution functions [34] with masses determined by the ratios $m_Z^2/m_t^2 = 23/83$ and $m_H^2/m_t^2 = 12/23$. We fix $m_t = 173.21$ GeV and $m_W = 80.379$ GeV, to 4 significant figures this yields $m_Z = 91.18$ GeV and $m_H = 125.1$ GeV. Our differential results are presented at a center-of-mass energy of $\sqrt{s} = 14$ TeV.

\sqrt{s}	LO [fb]	NLO [fb]
13 TeV	$52.42^{+25.5\%}_{-19.3\%}$	$103.8(3)^{+16.4\%}_{-13.9\%}$
13.6 TeV	$58.06^{+25.1\%}_{-19.0\%}$	$114.7(3)^{+16.2\%}_{-13.7\%}$
14 TeV	$61.96^{+24.9\%}_{-18.9\%}$	$122.2(3)^{+16.1\%}_{-13.6\%}$

Table 1: Total cross sections at LO and NLO with full top-quark mass effects, evaluated at scale $\mu_R = \mu_F = m_{ZH}$. The 7-point scale variation is also given.

We show results for the total cross section for $gg \rightarrow ZH$ at LO and NLO at various centre of mass energies in Table 1. The effect of the finite top-quark mass is fully included in our results. The quoted scale uncertainties are the result of a 7-point (renormalisation and factorisation) scale variation around the central scale of m_{ZH} . We find that the NLO QCD corrections are very large and enhance the LO cross section by roughly a factor of two. Going from LO to NLO the scale uncertainty is reduced by about a factor of 1.5. Our results agree, at the total cross section level, with those presented in Ref. [16], which were computed using an expansion around small m_H and m_Z .

In Figure 2 (left panel) we show differential results for the invariant mass distribution of the ZH system at LO and NLO at scale $\mu = \mu_R = \mu_F = m_{ZH}$ and $\mu = H_T = \sqrt{m_i^2 + p_{T,i}^2 + \sum_k |p_{T,k}|}$,

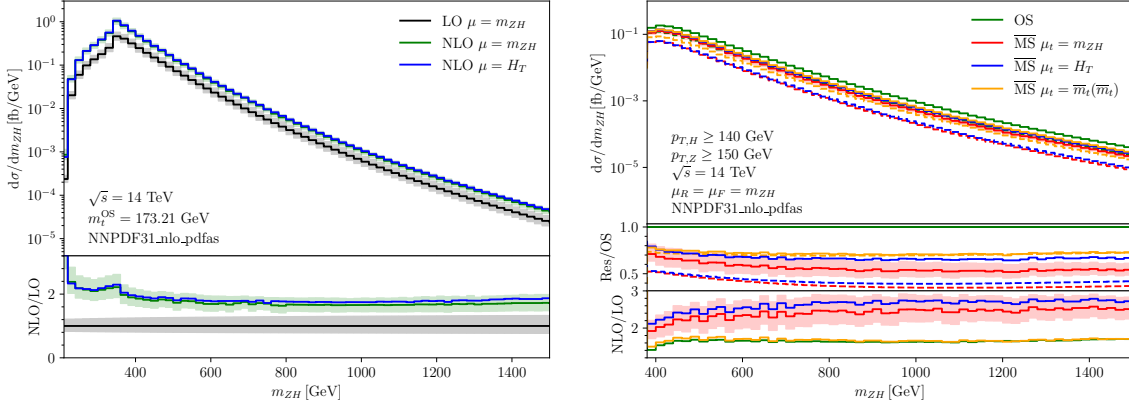


Figure 2: Invariant mass distribution for $gg \rightarrow ZH$ at LO and NLO. Left panel: fully inclusive results with $\mu = \mu_R = \mu_F = m_{ZH}$ or $\mu = H_T$ and the top-quark mass renormalised in the on-shell (OS) scheme. Right panel: results with cuts of $p_{T,H} \geq 140$ GeV, $p_{T,Z} \geq 150$ GeV shown for different choices of top-quark mass scheme and scale μ_t .

where the sum runs over all final state massless partons k . In the fully inclusive case, the NLO/LO K-factor is approximately two for most of the range and rises slowly at large invariant mass, it contains peaks at the $t\bar{t}$ and ZH production thresholds. In Figure 2 (right panel), we investigate the impact of the top-quark mass renormalisation scheme dependence on ZH production. After imposing the cuts $p_{T,H} \geq 140$ GeV, $p_{T,Z} \geq 150$ GeV, which select the moderate/high- p_T region, we display results in the on-shell (OS) scheme and the $\overline{\text{MS}}$ scheme. The top-quark renormalisation scale is set to $\mu_t = \{m_{ZH}, H_T, \bar{m}_t(\bar{m}_t)\}$, where $\bar{m}_t(\bar{m}_t)$ is the $\overline{\text{MS}}$ top quark mass at the scale of the $\overline{\text{MS}}$ top-quark mass. We observe that the choice of mass renormalisation scheme and scale has a significant impact on the result. For example, in the bin $m_{ZH} = [1000, 1020]$ GeV, at LO the $\overline{\text{MS}}(\mu_t = m_{ZH})$ result is 2.85 times the OS result, at NLO this ratio is reduced to 1.87.

In Figure 3 we show the transverse momentum of the Z-boson (left panel) and the Higgs boson (right panel) at LO and NLO. The band indicates the 7-point scale variation around the central scale choice of $\mu = m_{ZH}$ and the top-quark mass is renormalised in the on-shell (OS) scheme. We observe that even with the cuts $p_{T,H} \geq 140$ GeV, $p_{T,Z} \geq 150$ GeV, the NLO corrections are very significant at large p_T , enhancing the differential cross section by a factor of ~ 3 (~ 6) at 1 TeV for the Z-boson (Higgs boson). The size of these corrections can be partially understood from the large real radiation contribution, which is dominated by new configurations (not present at Born level) in which a hard jet recoils against a relatively hard Higgs boson. Strikingly, the $p_{T,H}$ distribution is markedly different from the $p_{T,Z}$ distribution at NLO, again, this difference can be attributed to new configurations in the real contributions [7, 35]. In diagrams where both the Higgs boson and Z boson are radiated from a top-quark loop, the probability to radiate a “soft” Z boson (with a Higgs boson recoiling against a hard jet) is related to the soft Eikonal factor $p^\mu / (p \cdot p_Z)$, where p^μ generically denotes the radiator momentum. On the other hand, the probability to radiate a “soft” Higgs boson is proportional to $m_t / (p \cdot p_H)$. The ratio of the two Eikonal factors is $\simeq p_T / m_t \gg 1$, thus it is more likely that the Z boson is soft and the Higgs boson is hard. For further discussion of our differential results, we refer the reader to Ref. [30].

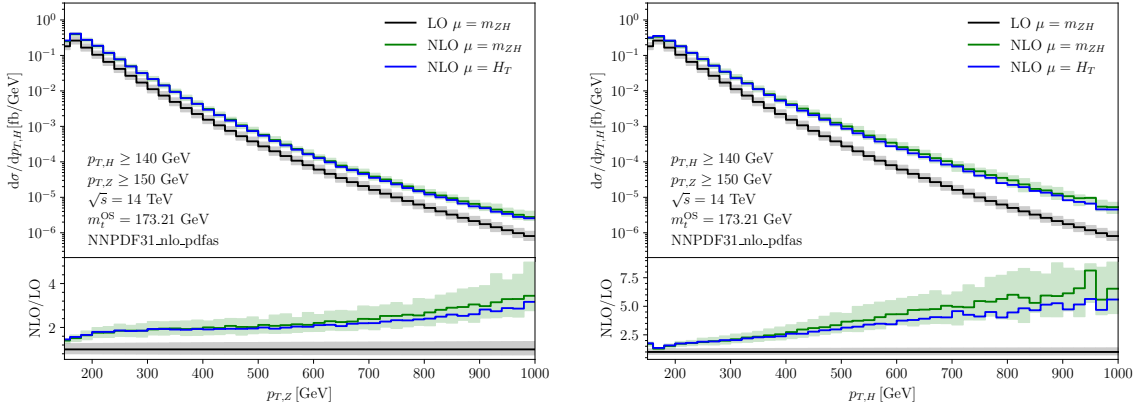


Figure 3: Left panel: Distribution of the Z-boson transverse momentum at LO and NLO. Right panel: Distribution of the Higgs boson transverse momentum at LO and NLO.

4. Summary

We have presented the complete two-loop NLO QCD corrections to the loop-induced process $gg \rightarrow ZH$. The NLO corrections increase the gluon fusion cross section by about a factor of 2, and reduce the scale dependence. Thus, at N^3 LO, the gluon channel is expected to account for around 10% of the $pp \rightarrow ZH$ total cross section. The inclusion of the NLO corrections to $gg \rightarrow ZH$ is essential for correctly describing ZH production at the LHC and HL-LHC. At large transverse momentum, the NLO corrections can be very large, more than 10 times the LO result for $p_{T,H}$. The large corrections can be traced back to the real radiation contribution which is enhanced when a soft Z boson is radiated from a top quark loop. We have also found that the choice of mass renormalisation scheme and scale for the top-quark mass is important. The difference between results in the $\overline{\text{MS}}$ scheme and the on-shell (OS) scheme remains at least as large as the usual renormalisation and factorisation scale uncertainties at NLO.

Acknowledgements

I would like to thank Long Chen, Joshua Davies, Gudrun Heinrich, Matthias Kerner, Go Mishima, Johannes Schlenk and Matthias Steinhauser for their collaboration on the original work summarised here. This work is supported in part by a Royal Society University Research Fellowship (Grant URF/R1/201268) and by the UK Science and Technology Facilities Council (STFC) through grant ST/T001011/1.

References

- [1] CMS collaboration, A. M. Sirunyan et al., *A search for the standard model Higgs boson decaying to charm quarks*, *JHEP* **03** (2020) 131 [[1912.01662](#)].
- [2] ATLAS collaboration, G. Aad et al., *Direct constraint on the Higgs-charm coupling from a search for Higgs boson decays into charm quarks with the ATLAS detector*, [2201.11428](#).

- [3] CMS collaboration, *Search for Higgs boson decay to a charm quark-antiquark pair in proton-proton collisions at $\sqrt{s} = 13$ TeV*, [2205.05550](#).
- [4] ATLAS collaboration, M. Aaboud et al., *Observation of $H \rightarrow b\bar{b}$ decays and VH production with the ATLAS detector*, *Phys. Lett. B* **786** (2018) 59 [[1808.08238](#)].
- [5] CMS collaboration, A. M. Sirunyan et al., *Observation of Higgs boson decay to bottom quarks*, *Phys. Rev. Lett.* **121** (2018) 121801 [[1808.08242](#)].
- [6] C. Englert, M. McCullough and M. Spannowsky, *Gluon-initiated associated production boosts Higgs physics*, *Phys. Rev. D* **89** (2014) 013013 [[1310.4828](#)].
- [7] B. Hespel, F. Maltoni and E. Vryonidou, *Higgs and Z boson associated production via gluon fusion in the SM and the 2HDM*, *JHEP* **06** (2015) 065 [[1503.01656](#)].
- [8] D. Goncalves, F. Krauss, S. Kuttimalai and P. Maierhöfer, *Higgs-Strahlung: Merging the NLO Drell-Yan and Loop-Induced 0+1 jet Multiplicities*, *Phys. Rev. D* **92** (2015) 073006 [[1509.01597](#)].
- [9] F. F. Freitas, C. K. Khosa and V. Sanz, *Exploring the standard model EFT in VH production with machine learning*, *Phys. Rev. D* **100** (2019) 035040 [[1902.05803](#)].
- [10] D. A. Dicus and C. Kao, *Higgs Boson - Z^0 Production From Gluon Fusion*, *Phys. Rev. D* **38** (1988) 1008.
- [11] B. A. Kniehl, *Associated Production of Higgs and Z Bosons From Gluon Fusion in Hadron Collisions*, *Phys. Rev. D* **42** (1990) 2253.
- [12] L. Altenkamp, S. Dittmaier, R. V. Harlander, H. Rzehak and T. J. E. Zirke, *Gluon-induced Higgs-strahlung at next-to-leading order QCD*, *JHEP* **02** (2013) 078 [[1211.5015](#)].
- [13] A. Hasselhuhn, T. Luthe and M. Steinhauser, *On top quark mass effects to $gg \rightarrow ZH$ at NLO*, *JHEP* **01** (2017) 073 [[1611.05881](#)].
- [14] J. Davies, G. Mishima and M. Steinhauser, *Virtual corrections to $gg \rightarrow ZH$ in the high-energy and large- m_t limits*, *JHEP* **03** (2021) 034 [[2011.12314](#)].
- [15] L. Chen, G. Heinrich, S. P. Jones, M. Kerner, J. Klappert and J. Schlenk, *ZH production in gluon fusion: two-loop amplitudes with full top quark mass dependence*, *JHEP* **03** (2021) 125 [[2011.12325](#)].
- [16] G. Wang, X. Xu, Y. Xu and L. L. Yang, *Next-to-leading order corrections for $gg \rightarrow ZH$ with top quark mass dependence*, [2107.08206](#).
- [17] L. Alasfar, G. Degrandi, P. P. Giardino, R. Gröber and M. Vitti, *Virtual corrections to $gg \rightarrow ZH$ via a transverse momentum expansion*, *JHEP* **05** (2021) 168 [[2103.06225](#)].
- [18] L. Bellafronte, G. Degrandi, P. P. Giardino, R. Gröber and M. Vitti, *Gluon Fusion Production at NLO: Merging the Transverse Momentum and the High-Energy Expansions*, [2202.12157](#).

- [19] G. Degrossi, R. Gröber, M. Vitti and X. Zhao, *On the NLO QCD Corrections to Gluon-Initiated ZH Production*, [2205.02769](#).
- [20] R. V. Harlander, S. Liebler and T. Zirke, *Higgs Strahlung at the Large Hadron Collider in the 2-Higgs-Doublet Model*, *JHEP* **02** (2014) 023 [[1307.8122](#)].
- [21] W. Bizoń, F. Caola, K. Melnikov and R. Röntsch, *Anomalous couplings in associated VH production with Higgs boson decay to massive b quarks at NNLO in QCD*, *Phys. Rev. D* **105** (2022) 014023 [[2106.06328](#)].
- [22] R. Gauld, A. Gehrmann-De Ridder, E. W. N. Glover, A. Huss and I. Majer, *VH + jet production in hadron-hadron collisions up to order α_s^3 in perturbative QCD*, *JHEP* **03** (2022) 008 [[2110.12992](#)].
- [23] CMS collaboration, A. M. Sirunyan et al., *Search for the associated production of the Higgs boson and a vector boson in proton-proton collisions at $\sqrt{s} = 13$ TeV via Higgs boson decays to τ leptons*, *JHEP* **06** (2019) 093 [[1809.03590](#)].
- [24] ATLAS collaboration, G. Aad et al., *Measurement of the associated production of a Higgs boson decaying into b-quarks with a vector boson at high transverse momentum in pp collisions at $\sqrt{s} = 13$ TeV with the ATLAS detector*, *Phys. Lett. B* **816** (2021) 136204 [[2008.02508](#)].
- [25] ATLAS collaboration, G. Aad et al., *Measurements of WH and ZH production in the $H \rightarrow b\bar{b}$ decay channel in pp collisions at 13 TeV with the ATLAS detector*, *Eur. Phys. J. C* **81** (2021) 178 [[2007.02873](#)].
- [26] ATLAS collaboration, *Combination of measurements of Higgs boson production in association with a W or Z boson in the $b\bar{b}$ decay channel with the ATLAS experiment at $\sqrt{s} = 13$ TeV*, tech. rep., CERN, Geneva, Sep, 2021.
- [27] ATLAS collaboration, *Measurement of the fiducial and differential cross-section of WH/ZH production for the b-jets + E_T^{miss} final state in pp collisions at $\sqrt{s} = 13$ TeV with the ATLAS detector*, .
- [28] G. Cullen, N. Greiner, G. Heinrich, G. Luisoni, P. Mastrolia, G. Ossola et al., *Automated One-Loop Calculations with GoSam*, *Eur. Phys. J. C* **72** (2012) 1889 [[1111.2034](#)].
- [29] G. Cullen et al., *GOSAM-2.0: a tool for automated one-loop calculations within the Standard Model and beyond*, *Eur. Phys. J. C* **74** (2014) 3001 [[1404.7096](#)].
- [30] L. Chen, J. Davies, G. Heinrich, S. P. Jones, M. Kerner, G. Mishima et al., *ZH production in gluon fusion at NLO in QCD*, [2204.05225](#).
- [31] S. Borowka, N. Greiner, G. Heinrich, S. P. Jones, M. Kerner, J. Schlenk et al., *Full top quark mass dependence in Higgs boson pair production at NLO*, *JHEP* **10** (2016) 107 [[1608.04798](#)].

- [32] S. Borowka, N. Greiner, G. Heinrich, S. P. Jones, M. Kerner, J. Schlenk et al., *Higgs Boson Pair Production in Gluon Fusion at Next-to-Leading Order with Full Top-Quark Mass Dependence*, *Phys. Rev. Lett.* **117** (2016) 012001 [[1604.06447](#)].
- [33] S. Catani and M. H. Seymour, *A General algorithm for calculating jet cross-sections in NLO QCD*, *Nucl. Phys. B* **485** (1997) 291 [[hep-ph/9605323](#)].
- [34] NNPDF collaboration, R. D. Ball et al., *Parton distributions from high-precision collider data*, *Eur. Phys. J. C* **77** (2017) 663 [[1706.00428](#)].
- [35] S. Amoroso et al., *Les Houches 2019: Physics at TeV Colliders: Standard Model Working Group Report*, in *11th Les Houches Workshop on Physics at TeV Colliders: PhysTeV Les Houches*, 3, 2020, [2003.01700](#).